

# Local Phase Tensor Features for 3-D Ultrasound to Statistical Shape+Pose Spine Model Registration

Ilker Hacihaliloglu\*, Abtin Rasoulia, *Student Member, IEEE*, Robert N. Rohling, *Senior Member, IEEE*, and Purang Abolmaesumi, *Senior Member, IEEE*

**Abstract**—Most conventional spine interventions are performed under X-ray fluoroscopy guidance. In recent years, there has been a growing interest to develop nonionizing imaging alternatives to guide these procedures. Ultrasound guidance has emerged as a leading alternative. However, a challenging problem is automatic identification of the spinal anatomy in ultrasound data. In this paper, we propose a local phase-based bone feature enhancement technique that can robustly identify the spine surface in ultrasound images. The local phase information is obtained using a gradient energy tensor filter. This information is used to construct local phase tensors in ultrasound images, which highlight the spine surface. We show that our proposed approach results in a more distinct enhancement of the bone surfaces compared to recently proposed techniques based on monogenic scale-space filters and logarithmic Gabor filters. We also demonstrate that registration accuracy of a statistical shape+pose model of the spine to 3-D ultrasound images can be significantly improved, using the proposed method, compared to those obtained using monogenic scale-space filters and logarithmic Gabor filters.

**Index Terms**—Gradient energy tensor, image registration, local phase, spinal injection, statistical shape model, ultrasound.

## I. INTRODUCTION

**B**ACK pain is the leading cause of disability in Americans under 45 years old. More than 26 million Americans between the ages of 20–64 experience frequent back pain [1]. The burden of back pain on the United States economy has been reported to be as high as \$62 billion [2]. In a recent study it has been reported that in European Union countries the cost for back pain management is estimated to exceed 12 billion Euros [3]. Forms of back pain management typically involve

physical therapy and oral medication. However, 20% of the patients treated with oral medication do not respond well to this treatment method [4]. In these situations, epidural steroid injections and facet joint injections have been employed in the treatment of back pain. The current protocols for guiding such procedures are based on fluoroscopy and computed tomography (CT). However, radiological needle guidance for analgesia delivery has significant drawbacks, particularly the use of ionizing radiation and the need for a specialized pain management clinic with access to fluoroscopy or CT. Furthermore, needle insertion and target localization is a fully 3-D problem, and one of the limitations of fluoroscopy-based systems is the difficulty in interpreting and using 2-D projection images to decide on the puncture site, needle trajectory, and depth of insertion.

Recently, a number of solutions have been proposed with the goal of reducing the radiation dose and increasing the needle placement accuracy, while maintaining or improving patient safety and reducing the complication rates. In search of a more accessible, portable, less expensive, more efficient, and nonionizing imaging alternative, ultrasound (US) guidance has enjoyed a growing interest. For example, researchers are looking into pre-puncture US to measure the depth from skin to epidural space [5] and for real-time guidance of needle insertion [6], [7]. Despite these recent developments, US has not become the standard-of-care for pain management because of issues related to poor quality depiction of anatomical landmarks, poor needle visibility, and the difficulty in interpreting images by inexperienced US operators (i.e., many anesthesiologists). These inherent limitations of US imaging are even more pronounced in the case of obese patients, in whom the greater distance from skin to target leads to lower image quality at the target location.

To overcome some of these problems and provide improved guidance, US images have been registered to a virtual representation of anatomical targets obtained from pre-procedure data such as CT or statistical shape models (SSMs) (e.g., [8]–[17]). Accurate, automatic, fast, and robust registration is critical for effective US-guided spine interventions.

Intensity-based registration approaches were proposed in [10]–[15]. Penney *et al.* [10] presented a CT-US registration approach where the US images were converted into probability images with bone surfaces representing higher probability. The method was evaluated in a cadaver study showing good accuracy and robustness. However, the probability images were generated from manual pre-segmented data which makes the method sensitive to the segmentation quality. Brendel *et al.* [11] segmented bone surfaces from CT data using US transducer

Manuscript received May 12, 2014; revised June 12, 2014; accepted June 17, 2014. Date of publication June 26, 2014; date of current version October 28, 2014. This study was jointly supported by grants from the Natural Sciences and Engineering Research Council of Canada (NSERC), Canadian Institutes of Health Research (CIHR), and the Institute for Computing, Information and Cognitive Systems (ICICS) at the University of British Columbia (UBC). Asterisk indicates corresponding author.

\*I. Hacihaliloglu is with the Department of Electrical and Computer Engineering, University of British Columbia, Vancouver, BC, V6T 1Z4 Canada (e-mail: ilkerh@ece.ubc.ca).

A. Rasoulia and P. Abolmaesumi are with the Department of Electrical and Computer Engineering, University of British Columbia, Vancouver, BC, V6T 1Z4 Canada (e-mail: purang@ece.ubc.ca).

R. N. Rohling is with the Department of Electrical and Computer Engineering, University of British Columbia, Vancouver, BC, V6T 1Z4 Canada, and also with the Department of Mechanical Engineering, University of British Columbia, Vancouver, BC, V6T 1Z4 Canada.

Color versions of one or more of the figures in this paper are available online at <http://ieeexplore.ieee.org>.

Digital Object Identifier 10.1109/TMI.2014.2332571

orientation information and registered these bone surfaces to *in vivo* US scans using an intensity-based registration method. The method was validated on *ex vivo* human lumbar spine. Winter *et al.* [13] validated the same method on *in vivo* datasets. The US datasets that had bone surfaces not clearly visualized were excluded from the study [13]. Yan *et al.* [12] extracted the posterior vertebral surface from CT by forward scan line tracing. US bone surfaces were extracted using a backward scan line tracing method. Registration was achieved using normalized cross correlation. Before US scanning, a surgical cavity filled with surgical saline, similar to that in an open-back surgery, was created in porcine cadavers. Although cadaver study results were successful creating a surgical cavity simplifies the imaging of the bone surfaces since the artifacts caused by the soft tissue interface are not present in the US scans. The reported registration time was 2 min. Gill *et al.* [14] simulated US images from CT data. These simulated US images were then registered to B-mode US scans using an intensity-based registration algorithm. Sheep cadaver setups and patient-based phantom models were used during the validation process. The authors reported a mean GPU registration time of 4 min. Khalilagh *et al.* [15] later extended this method and simulated US scans from SSM and registered them to US scans obtained from a phantom model. Although clinically acceptable registration results were achieved, the success rate is highly dependent on the acquired US scans, specifically on the intensity profile of the bone surface. The reported registration time was in the order of hours.

Point-based registration algorithms [16]–[18] were developed to improve the registration time. Baratt *et al.* [17] proposed a point-based registration method between CT and US that simultaneously determined the calibration parameters for a freehand 3-D US system. However, the bone surfaces were extracted manually, which is prohibitively time consuming, tedious and prone to significant inter- and intra-observer variability. In order to provide more robust and fast registration solutions automatic bone segmentation algorithms using intensity information were developed [19]–[21]. In [16] a dynamic programming approach [21] was used to segment bone surfaces from US data. These segmented surfaces were then registered to the CT dataset using an unscented Kalman filter (UKF) based surface registration approach [22]. Validation studies were performed on tissue mimicking phantoms created from a human spine and sheep cadaver. In recent work Rasoulia *et al.* [18] registered a statistical multi-vertebrae shape+pose model of the spine to *in vivo* US images using a Gaussian mixture model (GMM) based algorithm [23]. Spine surfaces were extracted from US data using a modification of the intensity-based dynamic programming algorithm developed by Foroughi *et al.* [21]. The main challenge in intensity-based bone segmentation techniques is the sensitivity of these techniques to US artifacts, algorithm parameters and machine settings affecting the accuracy of the proposed registration techniques. The typical high intensity bone surface response changes its intensity profile in situations where the US transducer is not oriented perpendicularly to the bone surface [19]. In the case of imaging highly curved bone surfaces, such as the vertebrae, this issue becomes

more problematic. In other words, the complex vertebral shape produces high variability in the angle of reflection to the US beam, which results in low contrast, blurred, and disconnected bone features.

To alleviate some of the challenges of bone extraction approaches, local phase-based US image enhancement methods were developed [24]–[31]. Local phase information was obtained by multiplying the US image data in frequency domain with 2-D/3-D Log-Gabor or monogenic filters. The output of this filtering operation was used to construct a local phase-based feature descriptor called phase symmetry (*PS*) or phase asymmetry (*PAS*) depending on the image edge feature type to be enhanced (e.g., a step edge for soft tissue or a ridge edge for bone) [24]–[31]. Promising results for accurately localizing soft tissue interfaces [24]–[28] and bone surfaces [29]–[31] from 2-D and 3-D US data were reported. In a recent work, Brounstein *et al.* [32] proposed a GMM based registration approach where bone surfaces were extracted using *PS* descriptor. The validation was performed on *in vivo* human pelvic US scans. Although such methods are intensity invariant, their success highly depends on the optimization of the filter parameters [30]. Furthermore, due to the complex shape of the vertebra the bone surface response profile will be composed of multiple edge features violating the assumption that using a single edge descriptor is sufficient for enhancement of anatomical features [33].

In summary, automatic, accurate, and fast extraction of bone surfaces and difficulty in acquiring US images with sharp bone boundary interfaces is an ongoing limitation of current US-guided spine interventions, restricting its use as a standard imaging modality for pain management.

In this study, we propose a new fully automatic US bone surface enhancement method. It is based on the use of a gradient energy tensor (*GET*) filter to construct a new feature enhancement metric, which we call the local phase tensor (*LPT*), for enhancing bone features from 3-D US data. The tensor is constructed using an isotropic band-pass filtered image, its gradient and Hessian. The proposed metric acts as a general boundary indicator and provides improved bone surfaces compared to the previously presented state-of-the-art local phase image enhancement methods [28]–[30]. Our second contribution includes the validation of the proposed method on 120 US volumes obtained from 10 subjects. We introduce a shape model to the US registration strategy, based on the work of Rasoulia *et al.* [18], in the context of guiding spine interventions. To the best of our knowledge this is the first study on the spine US registration that reports on an *in vivo* dataset of this size. We show that, when using the proposed method, an improvement in the registration accuracy and robustness could be achieved compared to previously published local phase-based image enhancement methods obtained using the Log-Gabor [29], [30] and monogenic filters [28]. Finally, we investigate the affect of the *GET* filter parameters on the registration accuracy and provide insight on which parameter values provide robust results. A preliminary investigation of our approach was reported in Hacıhaliloglu *et al.* [33]. This manuscript significantly extends our previous work by providing a more detailed description of

the methodology and performance analysis on a larger *in vivo* data set.

## II. METHODS AND MATERIALS

### A. Local Phase Tensor (LPT) for Bone Surface Enhancement

In US bone image analysis, arguably the most classical processing tools are intensity/amplitude-based techniques, both in the spatial and frequency domains. Consequently, smoothing and differentiation have been the subjects of intense study for segmentation or enhancement of bone surfaces. However, amplitude-based methods are sensitive to intensity variations. In particular, this can be a source of serious error for processing US images of the bone. The intensity profile can change from one scan to the next one depending on the machine settings, bone depth from the skin, overlaying anatomy and the orientation of the US transducer with respect to the bone surface. This may considerably reduce the optimality of the intensity-based image processing methods in US imaging and lead to unpredictable responses in the region of the expected bone surface. After the publication of the local energy-based feature detection method [34], local phase feature extraction has been investigated extensively. This feature extraction method postulates that features can be defined and classified using their phase. This observation model has led to the development of a number of local phase-based feature detection algorithms for US image data [24]–[31]. Local phase information is obtained by convolving images with a pair of band-pass quadrature filters. A common choice for US image processing is the Log-Gabor filter [26], [29] and the monogenic filter [27], [28]. The output of this convolution is used to construct phase-based descriptors such as *PS* for bone [29]–[31] and vein [28] localization, and *PAS* for border enhancement in echocardiography US images [26]. Successful results were obtained, but these descriptors are usually only valid for a single feature type (e.g., a step edge for soft tissue or a ridge edge for bone) and give no or wrong responses at points where the underlying feature model is violated. This is especially problematic in US scans of the spine where different boundary feature types are present due to the complex shape of the vertebrae and surrounding ligaments (Fig. 1). Investigating Fig. 1(b) we can see that the red scanline profile has two dominant ridge edge responses (shown with green arrows). The first ridge response (shown with thin green arrow) corresponds to the high intensity soft tissue interface shown in Fig. 1(a) with a corresponding thin green arrow. The second peak ridge response (shown with thick green arrow) corresponds to the expected location of the bone boundary as shown with a corresponding thick green arrow in Fig. 1(a). On the other hand, investigating the blue scanline profile, we can see that the ridge edge profile corresponding to the expected bone location [shown with thick magenta arrow in Fig. 1(a) and (b)] is not the dominant ridge response. For such an US image, using a descriptor optimized for ridge detection would result in the detection of correct as well as incorrect bone boundaries. In this work, we propose that an improvement can be achieved by moving from scalar feature descriptors to tensor-based ones where different feature response profiles can be detected together [Fig. 1(c)].

In order to compute local phase based features using tensor operators, we propose to use the GET filter. *GET* has shown to achieve better results compared to a structure tensor-based descriptor [35], [36] if simultaneous estimation of local orientation

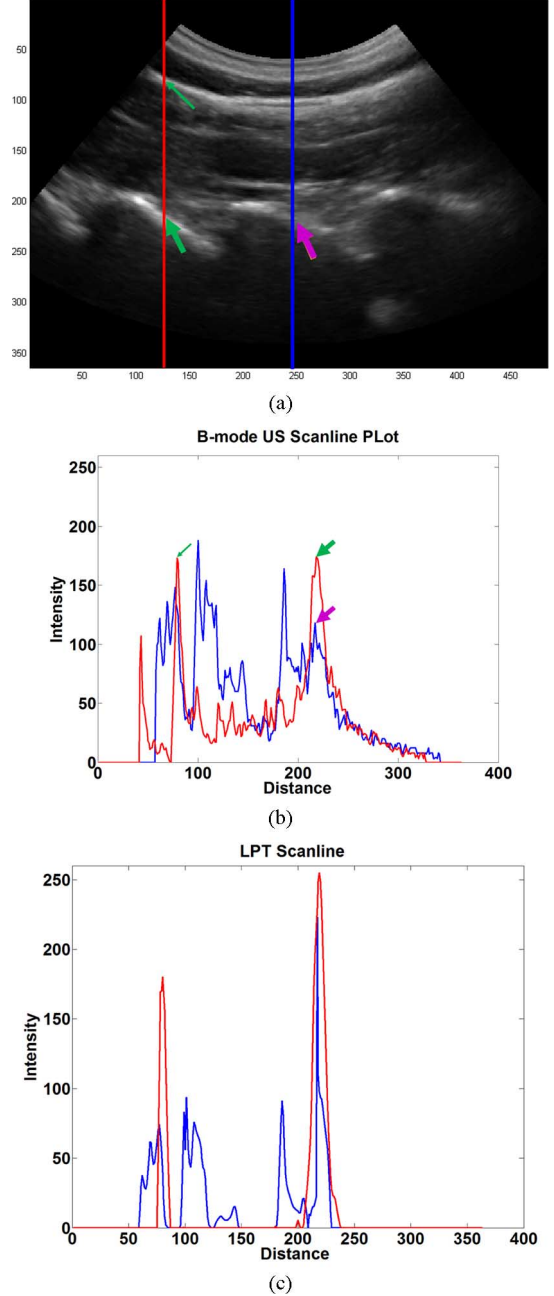


Fig. 1. (a) Paramedian 2-D B-mode US scan of the vertebrae lamina obtained *in vivo*. (b) Scanline profiles of the two (red and blue) vertical lines shown in (a) representing two different boundary feature types due to the complex shape of the vertebrae. Thin and thick green arrows point to the location of ridge edge features, with similar intensity values, that correspond to the soft tissue interface and bone boundary correspondingly. Thick magenta arrow points to the weak ridge edge feature corresponding to the expected bone boundary. (c) Corresponding scanline profiles extracted from the phase image obtained using the proposed LPT filter.

and phase information is required. The *GET* response is given as

$$\begin{aligned} GET(US_B(x, y)) \\ = T_{\text{even}} + T_{\text{odd}} = \begin{bmatrix} GET_{11} & GET_{12} & (1) \\ & GET_{21} & GET_{22} \end{bmatrix} \end{aligned}$$

where

$$\begin{aligned} T_{\text{even}} &= [\mathbf{H}(US_B(x, y))] [\mathbf{H}(US_B(x, y))]^T \\ T_{\text{odd}} &= -0.5 \times ([\nabla US_B(x, y)]) [\nabla^2 US_B(x, y)]^T \\ &\quad + [\nabla^2 US_B(x, y)] [\nabla US_B(x, y)]^T. \end{aligned} \quad (1)$$

The first term  $T_{\text{even}}$  represents symmetric features whereas the second term  $T_{\text{odd}}$  represents the asymmetric features.  $\mathbf{H}$ ,  $\nabla$  and  $\nabla^2$  denote the Hessian, Gradient, and Laplacian operations, respectively. In order to obtain localized frequency information and avoid the influence of the average grey level, we use a band-pass filtered version ( $US_B(x, y)$ ) instead of the original US image. For band-pass filtering of the B-mode US image, we use a Log-Gabor filter with a transfer function

$$G(\omega) = \exp \frac{-\log(\frac{\omega}{\kappa})^2}{2 \times \log(\sigma_\omega^2)}. \quad (2)$$

Here,  $\kappa$  is the center frequency of the filter and  $\sigma_\omega$  is related to the spread of the frequency spectrum in a logarithmic function. This filter is commonly applied in US image processing of bone and soft tissue interfaces [24], [26], [30]. The orientation representation  $\mathbf{z}$  and the orientation vector  $\mathbf{o}$  are given as  $\mathbf{z} = \lambda_1 - \lambda_2 = GET_{11} - GET_{22} + i2GET_{12}$  and  $\mathbf{o} = (\text{real}(\mathbf{z}^{0.5}), \text{imag}(\mathbf{z}^{0.5}))^T$ . Here, the superscript  $T$  denotes the transpose operation and  $\lambda_1$  and  $\lambda_2$  are the eigenvalues of the  $GET$ . The instantaneous phase information is calculated as

$$\varphi = \arg(s_{\text{even}} \sqrt{\text{trace}(T_{\text{even}})} + i s_{\text{odd}} \sqrt{\text{trace}(T_{\text{odd}})})$$

where

$$s_{\text{even}} = -\text{sign}(\mathbf{o}^T [\mathbf{H}US_B(x, y)] \mathbf{o})$$

and

$$s_{\text{odd}} = -\text{sign}(\mathbf{o}^T [\nabla US_B(x, y)]). \quad (3)$$

In monogenic signal analysis, the image is modeled as  $I(x, y) = A(x, y) \times \cos(\theta)$ , where  $A(x, y)$  represents the amplitude and  $\theta$  represents the phase. Based on this, we present a new phase metric called ( $LPT$ ) as

$$LPT(x, y) = \sqrt{T_{\text{even}}^2 + T_{\text{odd}}^2} \times \cos(\varphi). \quad (4)$$

The most important characteristic of this new metric is the tensor trace which is part of the instantaneous phase  $\varphi$  indicating the local contrast independently of feature type (edge, line, corner, or junction). Therefore, our new  $LPT$  acts as a general boundary indicator providing improved local phase features compared to the previously proposed state-of-the-art local phase methods obtained using the Log-Gabor filter [26], [29]–[31] and the monogenic filter [27], [28]. Since the previously proposed local phase methods were designed to extract a single type of feature (ridge or step edge), these methods can fail to enhance all of the bone features present in spine US images, where different feature types can correspond to the bone surface interface. The enhanced US images, using the  $LPT$  method, are used as an input to the registration method explained in the next section.

### B. Statistical Shape+Pose Multi-Bertebræ Model to Ultrasound Registration

In US-guided spine pain management procedures, to overcome the limitations in the depiction and interpretation of key anatomical features, US images have been registered with pre-procedure data. Accurate and robust registration is important for successful interventions. In this work, we investigate the augmentation of the US image data with a multi-vertebrae SSM which could be employed for procedures where pre-procedure CT data is not available. Our main aim is to show that the enhanced  $LPT$  features provide more accurate and robust registration results compared to the previously proposed local phase-based image enhancement methods [28]–[31].

For construction of the statistical multi-vertebrae shape+pose model, pose statistics are separated from the shape statistics since they are not necessarily correlated and do not belong to the same space. The method is based on the work of Rasouli *et al.* [18]. The reader is referred to Appendix A for a more detailed explanation of the construction of the model. Registration of the model to enhanced US images is performed using a GMM-based registration method [23]. In this iterative technique the previously generated model boundary points (moving point set, denoted as  $\mathbf{Z}$ ) are defined as the centroids of the GMM. The target,  $LPT$  bone surfaces (fixed point set, denoted as  $\mathbf{T}$ ), is considered to be an observation (data points) generated by the GMM.

During the registration process, soft-correspondences are established between the surface of the model and the target that is represented by a point set. Let us define the correspondence function for the  $n$ th point of the  $l$ th vertebra anatomy on the model, given as  $x_n^l$ , and the  $m$ th point of the target, given as  $y_m$ , as  $P(x_n^l, y_m)$  with a value between 0 and 1. The point set  $\mathbf{Y}$  constitutes a partial surface of the vertebrae extracted from the US images using the proposed  $LPT$  method. The intensity values of the  $LPT$  images are used as weights in this correspondence function. The model is instantiated and rigidly transformed to minimize the following cost function:

$$\begin{aligned} Q = \sum_{l=1}^L \sum_{m,n=1}^{M,N} P(x_n^l | y_m) &|| \mathbf{R} \Phi(x_n^l; \mathbf{w}^s, \mathbf{w}^p) + \mathbf{t} ||^2 \\ &+ \gamma^s \Gamma^s w^s + \gamma^p \Gamma^p w^p. \end{aligned} \quad (5)$$

The two latter terms are the regularization over the Principle Geodesics (PGs-see Appendix A) weights, and matrices  $\Gamma^s$  and  $\Gamma^p$  are, diagonal with elements  $1/\lambda^s$  and  $1/\lambda^p$ , the corresponding eigenvalues of the shape and pose of PGs, respectively.  $\mathbf{R}$  and  $\mathbf{t}$  are rotation and translation matrices representing the rigid transformation.  $w^s$  and  $w^p$  are the weights for the shape and pose models, respectively. The Quasi-Newton method is used during the optimization. Since all US volumes were acquired by placing the transducer at inter-vertebral levels 5–10 mm lateral to midline, an approximate location of the vertebrae is known *a priori*. This information is used to initialize the model during the registration. Note that the registration is performed based only on points of the model that are visible in US volumes, i.e., laminae, articular processes, and transverse processes. Fig. 2 shows the statistical shape+pose model of the L1-L5 vertebrae.

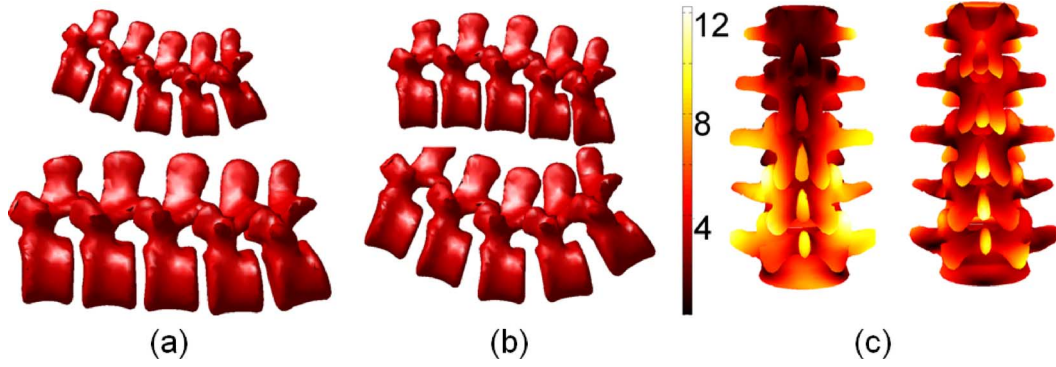


Fig. 2. Graphical representation of the L1-L5 vertebrae variations described by changing the weights corresponding to the first two principal modes of pose and shape variations by  $\pm 3\lambda^p$  and  $\pm 3\lambda^s$ , respectively, where  $\lambda^p$  and  $\lambda^s$  are the corresponding eigenvalues. First mode of pose variations represents mainly the scaling and the lateral curvature, and the second mode represents the anterior-posterior curvature of the spine. First and second modes of variation of shape represent variations in the transverse processes and vertebral body, respectively. (a) Pose first mode, (b) pose second mode, (c) shape first mode (left) and shape second mode (right), where the amount of shape variations are color coded on the mean shape.

### C. Data Acquisition

A total of 10 patients who provided informed consent were included in the validation experiments. In total 120 3-D US volumes were captured by an expert sonographer using a Sonix-Touch US machine (Ultrasonix, Medical Corp, Richmond, BC, Canada) with a curvilinear 3-D transducer (4D C7-3/40), operating at 3.3 MHz with depth of 7 cm. For each volume, 80 frames over a 60° field of view were captured. US volumes were acquired with each subject in the prone position. For each subject, the sonographer identified and marked the intervertebral levels (four in total L1-L2, L2-L3, L3-L4, and L4-L5) on the skin. In total, 12 3-D US volumes were acquired for each subject. Bone surfaces, representing anatomical landmarks, were then marked on the US images manually by the expert sonographer to provide a gold standard for the registration. These manually selected landmarks were chosen from the spinous process, and superior and inferior articular process of vertebra. Corresponding landmarks were also identified from the generated shape model. These landmarks were only used for validation and were not part of the registration process.

## III. EXPERIMENTS

In order to find optimum values for the Log-Gabor filter center frequency ( $\kappa$ ), frequency bandwidth ( $\sigma_\omega$ ) and standard deviation ( $\delta$ ) for calculating the Hessian, Gradient, and Laplacian, we performed an exhaustive search for various combinations of these parameters. The range of values used for  $\kappa$ ,  $\sigma_\omega$ , and  $\delta$  were [5 increment 10–70], [0.05 increment 0.1–0.7], and [0.05 increment 0.1–1], respectively. The statistical shape+pose multi-vertebrae model was registered to each *LPT* image obtained from the combination of the various parameter values. The target registration error (TRE) value was calculated as the root mean square (rms) distance between the manually selected landmarks from the US scans and the statistical shape model after the registration. This *LPT* filter parameter analysis was performed on 20 US volumes randomly chosen from the group of 120 volumes. The *LPT* filter parameters with the minimum TRE were used during the quantitative and qualitative validation experiments.

In order to compare the *LPT* filtering approach against the previously proposed state-of-the-art local phase filtering methods, the US images were also processed with the Log-Gabor filter-based *PS* descriptor [30] and the monogenic filter-based feature symmetry (*FS*) descriptor [28] before inputting them to the registration framework. The *PS* descriptor was constructed using the automatically optimized Log-Gabor filter parameters based on the work of Hacıhaliloğlu *et al.* [30]. The *FS* descriptor was constructed by performing an exhaustive search for various combinations of the frequency bandwidth ( $\sigma_\omega$ ) ([0.05 increment 0.1–0.7]) and filter center frequency ( $\kappa$ ) ([five increment 10–70]) parameters. We selected a single scale since using multiple scales does not improve the bone surface localization accuracy but adds extra computation time [31]. Again the *FS* filter parameters with the minimum TRE were used during the quantitative and qualitative validation experiments. A detailed formulation of the *PS* and *FS* methods are explained in Appendices B and C. The RMS distance error was calculated between the manually selected landmarks from the US scans and the statistical shape model after the registration. Two experiments were performed to evaluate the effectiveness of the proposed filtering methodology.

### A. Experiment 1

For qualitative evaluation of the proposed *LPT*-based bone filtering method, samples of processed *in vivo* 3-D US scans were manually annotated as the gold standard. Furthermore, we show qualitative comparison results between the bone surfaces extracted using the proposed method and the state-of-the-art Log-Gabor filter-based *PS* method [29], [30] and the monogenic filter-based *FS* method. Additionally, we present qualitative results by graphically displaying examples of the registered surfaces using the proposed method.

### B. Experiment 2

TRE results between the 120 *in vivo* US scans and the generated shape model are presented for quantitative evaluation. We also provide quantitative comparison results between the TRE results obtained using the previously proposed Log-Gabor filter



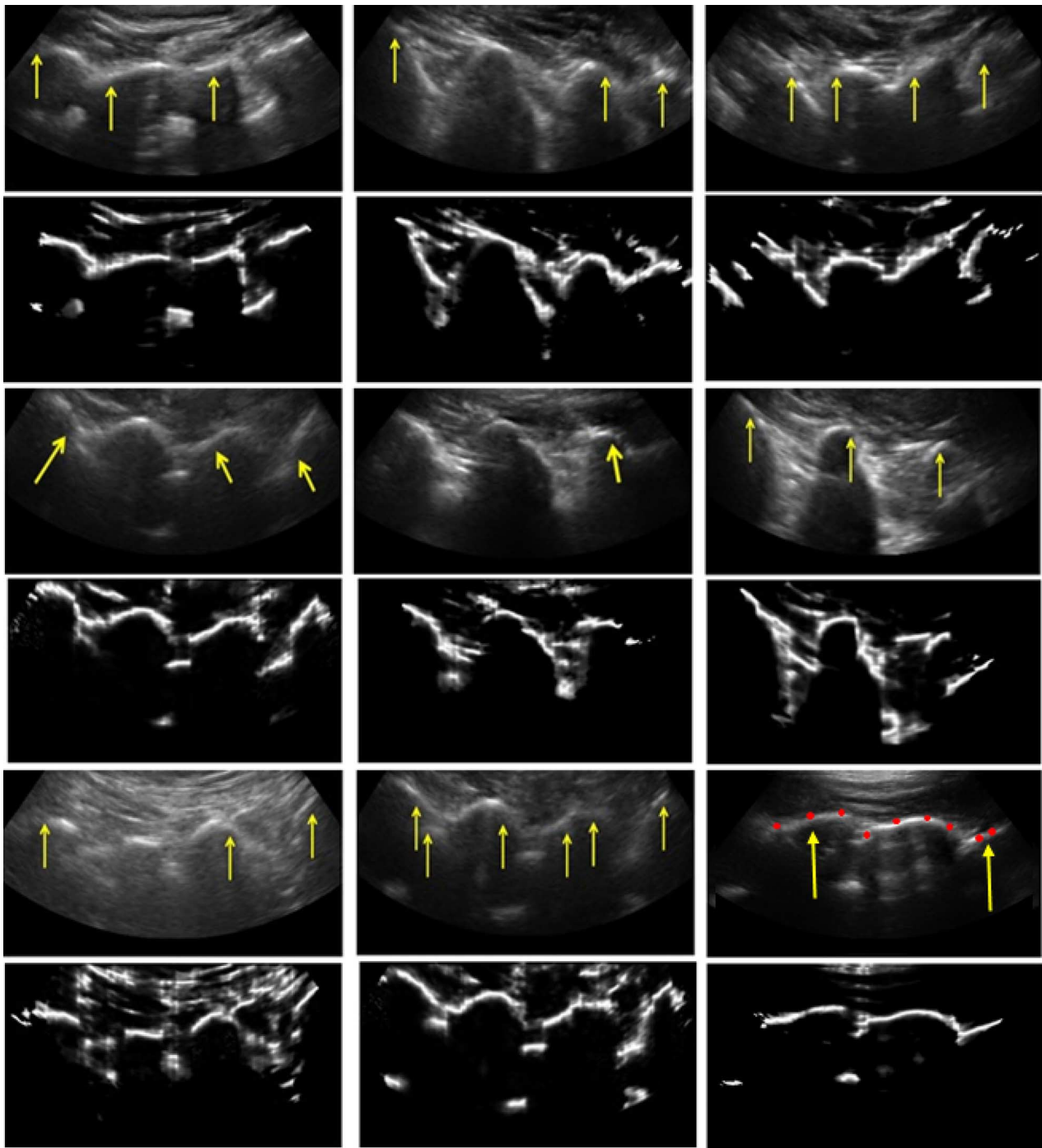


Fig. 3. Qualitative results obtained from clinical scans. First, third, and fifth rows: B-mode US images. Second, fourth, and sixth rows: Corresponding *LPT* images. Yellow arrows point to the locations where bone surface are low contrast and appear blurred. Bone surfaces appear sharper in *LPT* images. B-mode US image shown in row five last column is also displaying an example of the manually selected landmarks (red dots) used during the quantitative validation experiment.

based *PS* method [29], [30] and the monogenic filter based *FS* method.

#### IV. RESULTS

The proposed filtering, statistical shape+pose multi-vertebrae model generation and registration approaches were implemented in MATLAB and run on a 2.67 GHz Intel *Core i5* with 8 GB of RAM. The exhaustive parameter search resulted

in Log-Gabor filter center frequency of  $\kappa = 25$  pixels and frequency bandwidth value of  $\sigma_\omega = 0.25$ . Previously it has been shown that choosing similar filter parameters provided good bone surface localization results [29], [30]. The same exhaustive search provided a standard deviation value of  $\delta = 0.15$  pixels for calculating the Hessian, Gradient, and Laplacian. These values were not changed throughout the experimental validation.

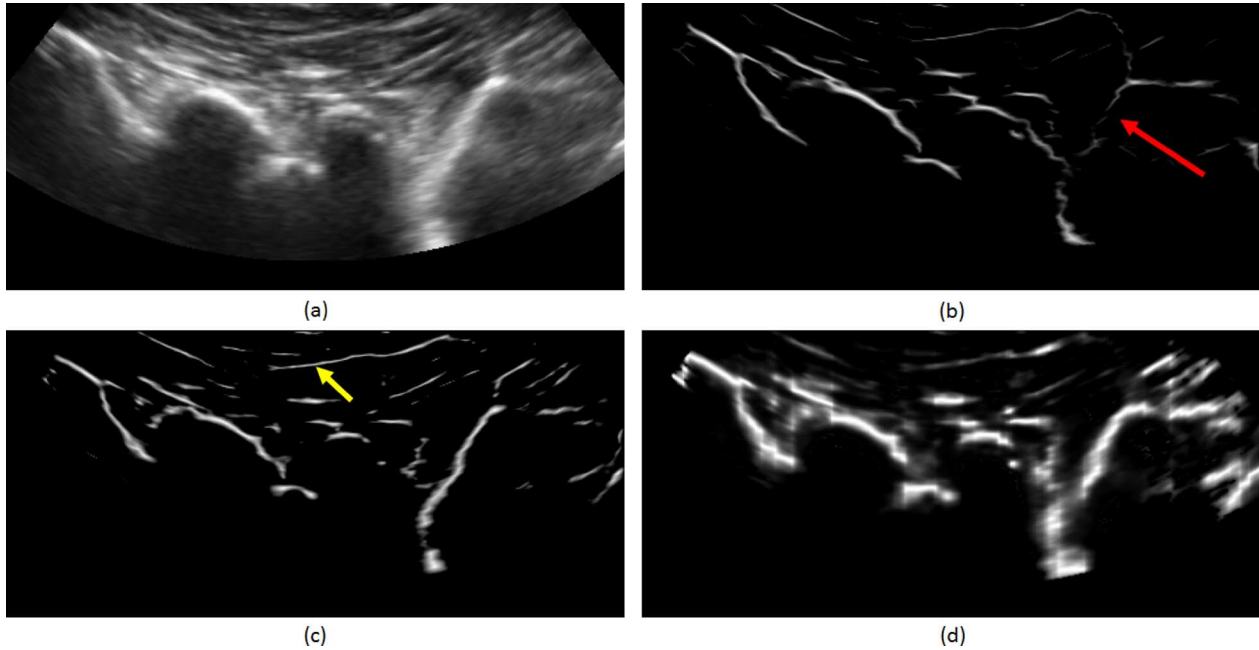


Fig. 4. Qualitative results for local phase based bone surface enhancement methods. (a) *In vivo* B-mode US image. (b) *PS* surface obtained using the method [30]. (c) *FS* surface obtained using the method [28]. (d) Proposed *LPT* surface. Red arrows point to the locations of the missing bone surface using the *PS* method. Yellow arrow points to the enhanced soft tissue interface with the *FS* method.

#### A. Experiment 1


Qualitative results obtained from *in vivo* scans are shown in Fig. 3. Due to the previously mentioned difficulties while imaging vertebrae, some of the lamina bone surfaces appear blurred or with low contrast (yellow arrows in Fig. 3). For these cases, the proposed *LPT* based method results in the extraction of sharper and higher contrast lamina bone surfaces, although some false positive results  also noted. The method appears unaffected by intensity variations present in different US scans.

Fig. 4 shows qualitative comparison results between the *LPT* based method and previously proposed Log-Gabor filter based *PS* and monogenic filter based *FS* methods. The *PS* method results in a missing vertebra surface shown with red arrow [Fig. 4(b)].

Investigating Fig. 4(a) we can see that the dominant (high intensity) features are oriented horizontally and along 145 degrees. The filter parameter optimization framework [30] used to construct the Log-Gabor filter, in order to obtain optimized *PS* features, is guided by the information obtained from the dominant features present in the US image. Therefore, during the optimization process the filtered is steered/oriented so that it is perpendicular to these dominant image features. Since the bone surface shown with the red arrow is not oriented horizontally or along 145°, it will be missed during the filter optimization process. On the other hand, the *FS* method enhances all bone surfaces with additional soft tissue artifacts shown with yellow arrow with similar intensity values as the enhanced bone surfaces. The *LPT* based method is least effected from the soft tissue artifacts and provides enhanced sharp bone boundaries with highest intensity values associated with bone boundaries.

Investigating Figs. 5 and 6 we can see that the *PS* and *FS* methods result in the enhancement of bone as well as soft tissue interfaces, where high intensity values are associated with all of

the enhanced features. Since both of these methods act as a ridge edge detector they enhance all the ridge features and assign similar high intensity values to the enhanced features. The proposed *LPT* method uses the combination of three different filter outputs to construct a general phase descriptor without being tuned to a specific edge type. Therefore, in comparison the proposed method results in the enhancement of bone features with highest intensity values associated with them (Figs. 5 and 6). This is a desired outcome since the intensity values of the enhanced local phase images are used as weights during the registration process. Having the enhanced high intensity features localized along the bone surface will guide the model to the correct location during the registration optimization. Qualitative results on registering statistical shape+pose multi-vertebrae model to the enhanced bone surfaces are presented in Fig. 7. We can see that the proposed method successfully aligns the two volumes (Fig. 7) where a close match between the two surfaces is visible.

#### B. Experiment 2

The processing time for the proposed method was 0.05 s for a 2-D US image compared to 6 s for the *PS* method [30] and 0.06 s for the *FS* method [28]. Registration of the statistical shape+pose multi-vertebrae model to US was achieved in 39 s. The registration results obtained with the proposed method were significantly better than the previously proposed *PS* and *FS* methods (paired t-test,  $p < 0.05$ ). The overall TRE calculated from the selected anatomical landmarks was  $2.0 \text{ mm} \pm 0.4 \text{ mm}$  for all the 120 scans with a maximum TRE value of 2.4 mm for registering L2-L3 and minimum TRE value of 1.8 mm for registering L3-L4. The maximum registration results for the L1-L2 and L4-L5 were 2.7 mm and 3.1 mm, respectively. The *FS* approach [28] obtained a TRE error value of  $3.2 \text{ mm} \pm 2.1 \text{ mm}$  (Table I). Maximum TRE was for the L2-L3 vertebral level with

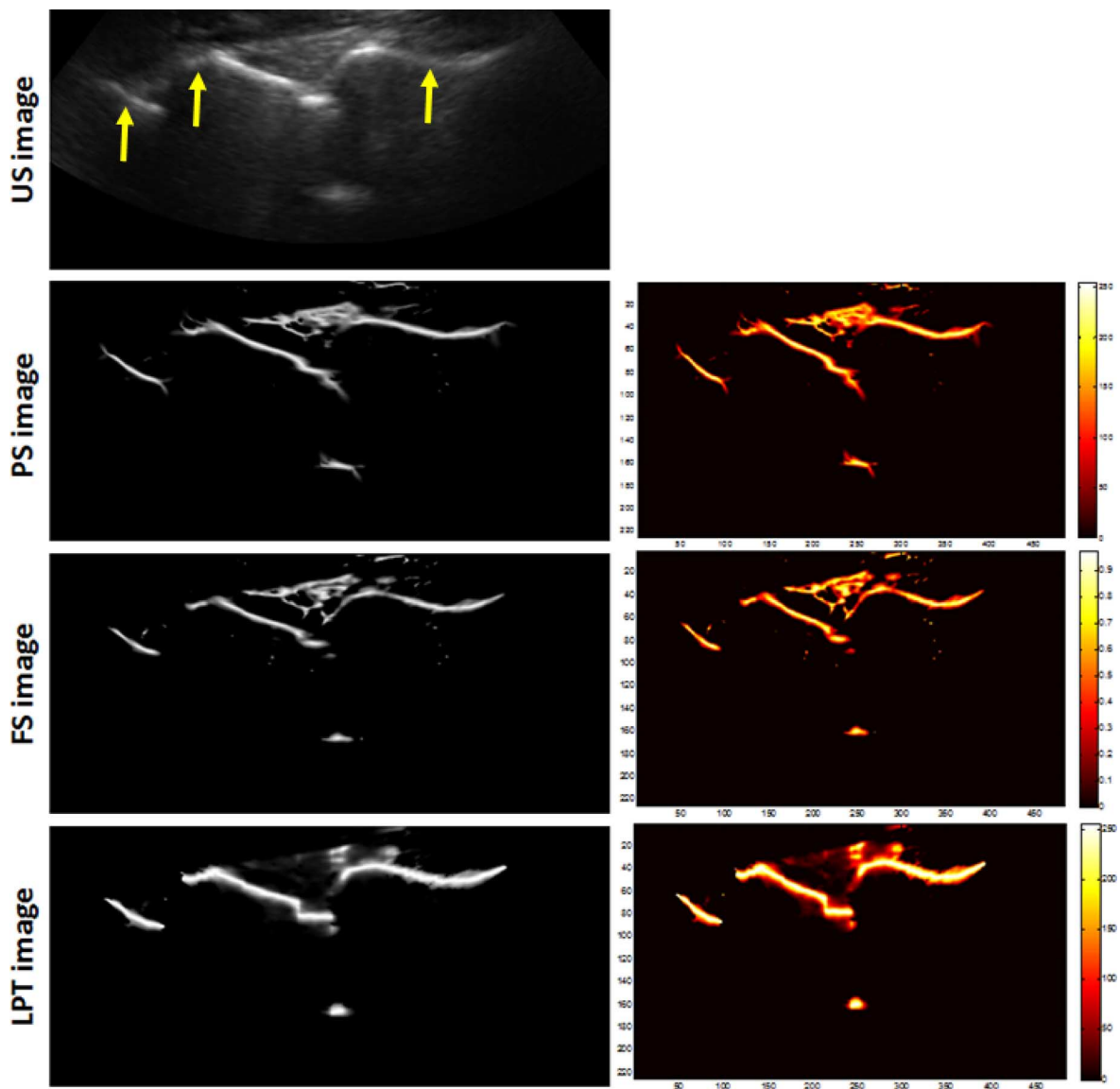


Fig. 5. Qualitative comparison results of the *PS*, *FS*, and *LPT* methods. First row: B-mode *in vivo* US image. Yellow arrows point to the locations where bone surface are low contrast and appear blurred. Second, third, and fourth rows: Corresponding *PS*, *FS*, and *LPT* images. Second column shows the color coding of the local phase surface images. Soft tissue interfaces are more enhanced using the previous *PS*, *FS* methods. Investigating the color coded images we can see that all the enhanced features, using the previously proposed methods, have high intensity pixels. In the proposed *LPT* method the highest intensity pixels belong mostly to the enhanced bone surfaces.

a value of 6.8 mm. The minimum TRE was obtained for the L3-L4 level (2.5 mm). The TRE results were the highest using the previously proposed PS filtering [30] method. This method achieved an overall TRE value of  $10.6 \text{ mm} \pm 9.1 \text{ mm}$ . Maximum TRE was for the L4-L5 level with a value of 25 mm and minimum TRE was obtained for the L3-L4 level with a value of 6.3 mm. L3-L4 level resulted in the lowest TRE for all the registrations obtained using the PS, FS, and the proposed LPT method.

Fig. 8 shows the effect of LPT filter parameters on the TRE. The plots are obtained using eight volumes (denoted as eight different colored lines) which were part of the exhaustive search filter parameter optimization process. For each plot, two of the filter parameters were fixed to the optimum value obtained from the exhaustive search process while the third parameter was changed. Investigating the plots we can see that for the eight

volumes most of the TRE values are below 2.6 mm even using nonoptimal filter parameter values.

## V. DISCUSSIONS AND CONCLUSION

Obtaining a clear depiction of bone surfaces in US images continues to be a challenging problem affecting the success of many US-guided interventions. Local phase image processing based on Log-Gabor filtering for bone enhancement has been reported in the past with successful results [29]–[31]. However, the phase metrics constructed previously are usually only valid for a single feature type and give no or wrong responses at points where the underlying feature model is violated. Furthermore, one is faced with the complexity of constructing oriented filter banks which makes the success of the proposed methods dependent on the selected orientations. Finally, orienting the



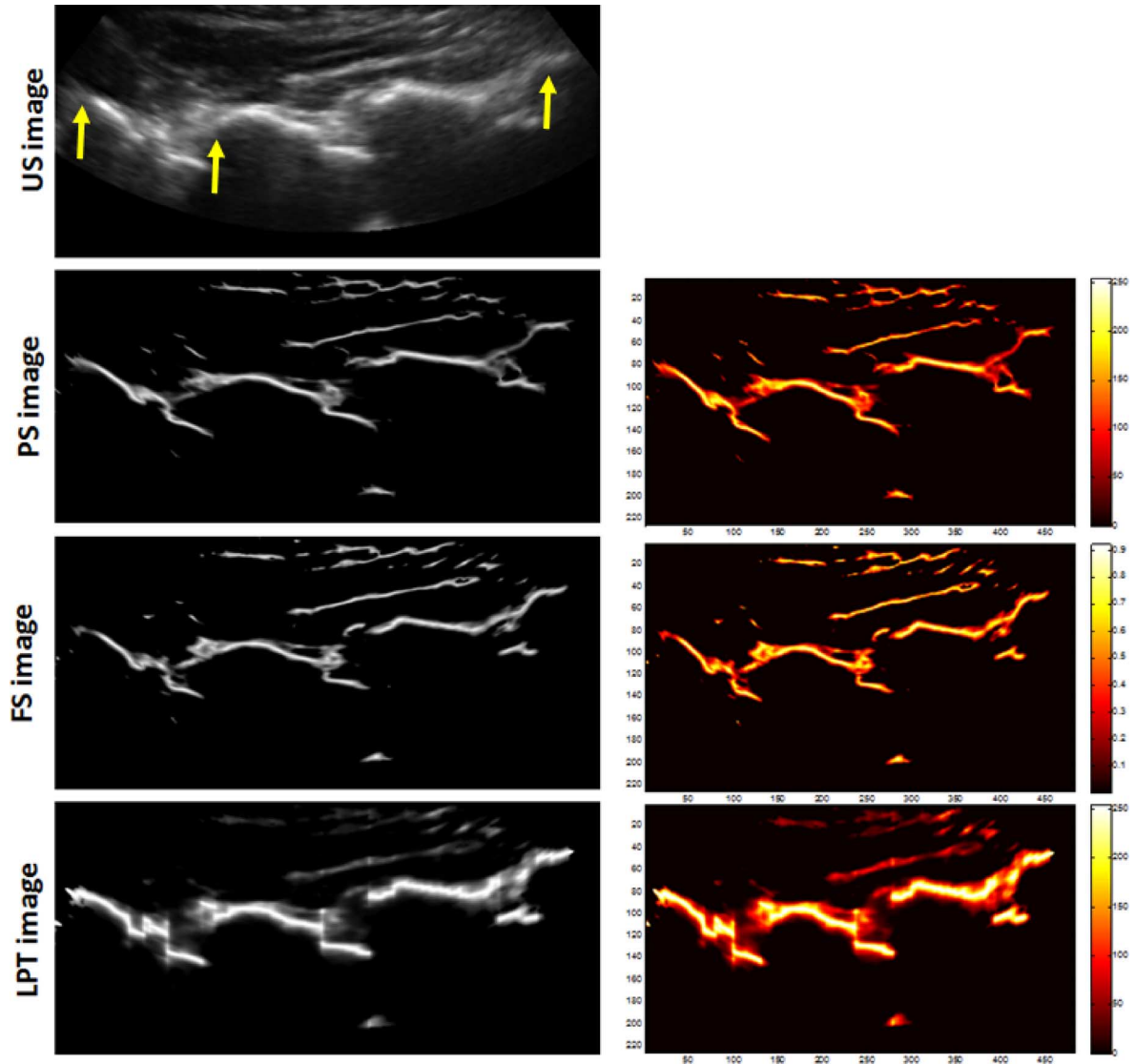


Fig. 6. Qualitative comparison results of the *PS*, *FS*, and *LPT* methods. First row: B-mode *in vivo* US image. Yellow arrows point to the locations where bone surface are low contrast and appear blurred. Second, third, and fourth rows: Corresponding *PS*, *FS*, and *LPT* images. Second column shows the color coding of the local phase surface images. Soft tissue interfaces are more enhanced using the previous *PS*, *FS* methods. Investigating the color coded images, we can see that all the enhanced features, using the previously proposed methods, have high intensity pixels. In the proposed *LPT* method, the highest intensity pixels belong mostly to the enhanced bone surfaces.

constructed filter to cover the whole frequency spectrum increases the computational time of these methods as well. On the other hand, monogenic filter based approaches [28] overcome the filter bank construction problem by being isotropic filters, however, the descriptors constructed using this filter are again only valid for a single feature type and face similar problems as the Log-Gabor filter.

In this paper, we provide solutions to these problems by proposing a new approach for enhancing spine bone surfaces from 3-D US data. The proposed method is based on the use of the gradient energy tensor filter for constructing a novel phase metric. The tensor is generated using an isotropic band-pass filtered image, its gradient, and Hessian. Moving from scalar based descriptors to tensor-based ones allows the extraction of multiple feature types which results in the enhancement of spine surfaces where different boundary feature types are present due to the complex shape of the vertebrae and liga-

ments. The enhanced bone features are then registered to a statistical shape+pose multi-vertebrae model constructed using a novel method where pose statistics are separated from the shape statistics.

Joint space width is approximately  $1.93 \pm 0.51$  mm [37]. The size of the epidural space in an adult measures about 7.5 mm in the upper thoracic region, 4.1 mm at T11–12 region, and 4–7 mm in the lumbar [38]. Given the size of the target, our achieved accuracy of approximately 2 mm should be sufficient to allow clinician guide the needle toward the facet joint with sufficient accuracy. We should note that throughout a procedure, we foresee that the needle insertion is monitored continuously by live ultrasound imaging, hence, any residual error in registration and guidance can be corrected as needle is inserted. The proposed method enhances the blurred and low contrast vertebrae surfaces from *in vivo* scans and achieves registration errors with a mean value of 2 mm. The proposed *LPT* based method

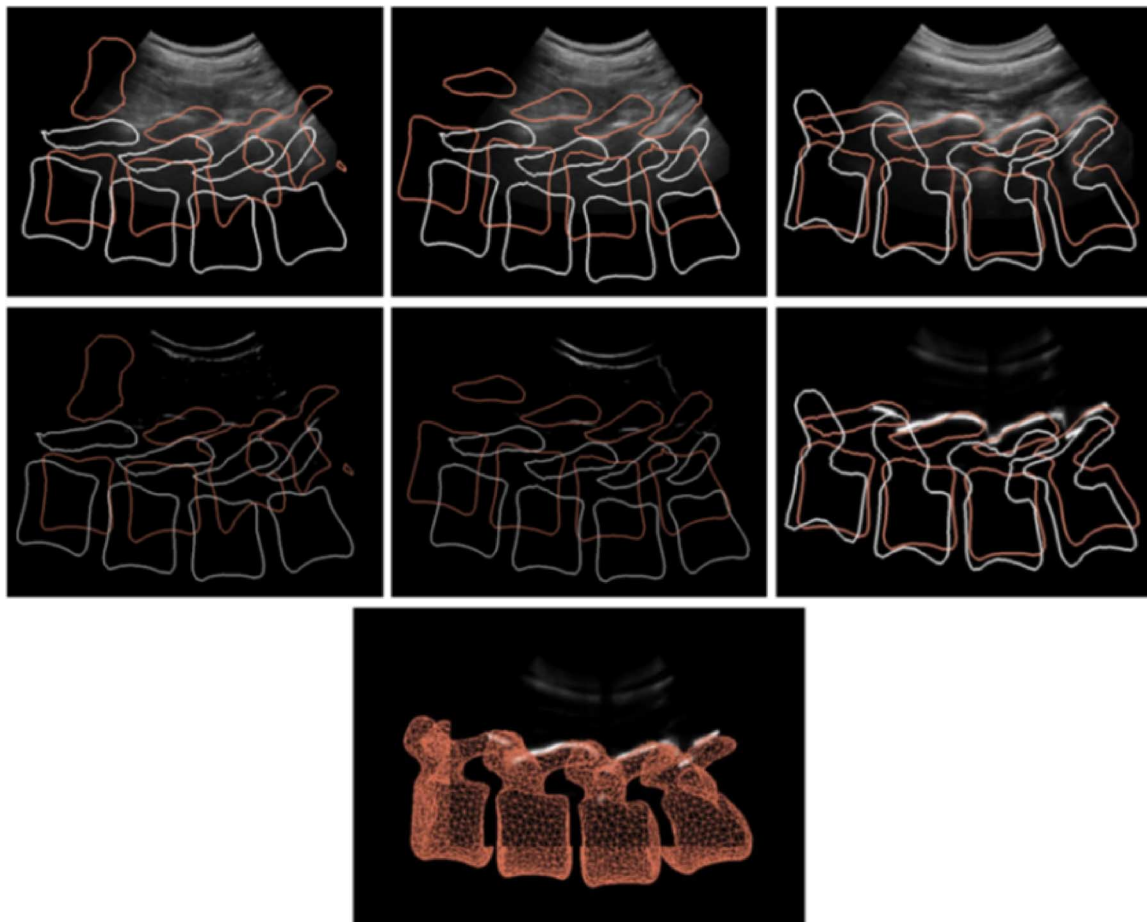


Fig. 7. Qualitative results for statistical shape+pose multi-vertebrae model to US registration. Initial position of the model (prior registration) is drawn in white and the registered statistical shape+pose multi-vertebrae model is in red. First row left to right: Overlay of *in vivo* B-mode US slice with the outline extracted from the statistical shape+pose multi-vertebrae model using the FS, PS, and LPT features. Second row left to right: Overlay of the FS, PS, and LPT features with the outlines extracted from the statistical shape+pose multi-vertebrae model. Third row: Overlay of the LPT features with the 3-D statistical shape+pose multi-vertebrae model after registration. Note that the intensity scale for the second row images is not normalized.

also achieved consistent registration results between different intervertebral levels suggesting the robustness of the method while imaging different regions of the vertebra. Furthermore, we obtain statistically significant improvements ( $p < 0.05$ ) in accuracy compared to previously proposed local phase methods. Qualitative results show that most of the high intensity features in the enhanced *LPT* images correspond to the bone surface interfaces. Since the registration is guided with the intensity values it results in improved TRE values compared to the *FS* and *PS* methods where high intensity features could be located in the enhanced soft tissue interfaces as well affecting the overall accuracy of the model to US registration. We also achieve improved registration results compared to state-of-the-art simulation-based SSM-US registration approaches [15], [18] where a TRE value of 3.48 mm was reported. The statistical shape+pose multi-vertebrae model construction and GMM registration algorithm presented in this study is based on the work of Rasoulian *et al.* [18]. In that study, the bone surfaces were extracted using an intensity-based bone enhancement method. Validation performed on 69 *in vivo* datasets achieved a mean rms value of 2.6 mm. In this study, we have proved that an improvement could be achieved by moving from an intensity based approach to a local phase based approach.

In computer assisted orthopaedic surgery registration of a statistical shape model to intra-operative fluoroscopy is a widely used method with reported accuracies of 1.2 mm and 2 mm depending on the target anatomy [39]. However, to the best of our knowledge, there are no reports for registering multi-vertebrae shape models. Furthermore, X-ray based methods subject the patient to ionizing radiation, which makes those methods less favorable. US based method do overcome the radiation exposure problem while achieving clinically acceptable registration results [8]–[17].

The computation time for the proposed filtering method is 0.05 s for a single 2-D B-mode US slice. The statistical shape+pose multi-vertebrae model to US registration was achieved in 39 s. Both methods were implemented in MATLAB which is typically an order of magnitude slower than a C++ implementation. To alleviate this problem and provide real-time guidance, the computation times could be further reduced by implementing the filtering and registration methods on a multi-processor graphic processing unit (GPU). The *LPT* filtering and processing of each US image can also be achieved using parallel computing. In a recent publication, Amir-khalili *et al.* [39] showed that PS filtering could be achieved in 74 ms for a cubic volume of size  $128^3$ . The improvement in the

TABLE I  
RESULTS OF STATISTICAL SHAPE+POSE MULTI-VERTEBRAE MODEL TO US REGISTRATION USING THE PROPOSED IMAGE ENHANCEMENT, AND PREVIOUS LOCAL PHASE FILTERING APPROACHES [28], [30]. LAST ROW INDICATES THE AVERAGE OF ALL rms REGISTRATION ERRORS FOR ALL SCANS (96) INCLUDED IN THE STUDY

	Proposed Method Mean (mm) $\pm$ SD (mm)	FS Method [28] Mean (mm) $\pm$ SD (mm)	PS Method [30] Mean (mm) $\pm$ SD (mm)
L1-L2	1.9 $\pm$ 0.5	3.3 $\pm$ 3.2	10.9 $\pm$ 9.2
L2-L3	2.4 $\pm$ 0.7	3.9 $\pm$ 2.9	13.9 $\pm$ 7.6
L3-L4	1.8 $\pm$ 0.3	2.1 $\pm$ 0.5	3.9 $\pm$ 2.4
L4-L5	2.0 $\pm$ 1.1	3.4 $\pm$ 1.6	14.0 $\pm$ 11.0
Total	2.0 $\pm$ 0.4	3.2 $\pm$ 2.1	10.6 $\pm$ 9.1

performance of the *PS* method is achieved by constructing the Log-Gabor filters offline and performing the convolution operation in the Fourier domain using element-wise multiplication [39]. Since filter creation and the convolution operation are also part of the proposed *LPT* based method similar approach could be used in order to achieve performance improvements.

The proposed *LPT* method processes each individual 2-D slice of a 3-D US volume. However, previously it was shown that 2-D US image processing methods are inherently limited to cross-sectional analysis and do not consider the continuity of the bone surface in the elevation direction [31]. Therefore, we are planning on extending the method to a full 3-D analysis. Moreover, we will validate the method on a larger clinical data set, and on different registration approaches for guiding spine injections.

#### APPENDIX A

##### STATISTICAL MULTI-VERTEBRAE SHAPE+POSE MODEL CONSTRUCTION

The variability of the patient's position and orientation, introduced during the data collection, will have an effect on the pose and shape statistics. Furthermore, the pose and shape statistics are not necessarily correlated and do not belong to the same space. Additionally, poses are represented transformations forming a Lie group, a Riemannian manifold, where analysis in Euclidean space is not applicable [40]. Thus, we construct a statistical model by separating pose statistics from shape statistics [41], [42]. In order to build statistics on the variability of data on a manifold we use principal geodesic analysis (PGA) which is a generalization of principal component analysis (PCA) on Euclidean spaces to non-Euclidean manifolds.

Principal geodesics (PG), are defined for Lie groups which provide the modes of variations. A Lie group  $G$  is a differentiable manifold and a group where multiplication and inversion are smooth. The tangent space at the identity element is called Lie algebra,  $\mathfrak{g}$ . To map elements from tangent space into a Lie group  $G$ , exponential mapping  $\mathfrak{g}: \exp(x) \rightarrow G$ , and its inverse logarithm mapping  $G: \log(x) \rightarrow \mathfrak{g}$  are used.

The approximation of PGs are as follows. Initially, the transformations  $T_i$  are transformed to a tangent space at the average transformation,  $\mu$ , by logarithmic mapping:  $\log_\mu T_i$  [40]. Here,  $i$  represents the number of elements. Next, PCA is applied and lastly, principle components  $\nu_l$  are transformed back to the original space by exponential mapping:  $\exp_\mu(\nu_l)$ .

If the training set contains  $N$  instances of a group of  $L$  vertebrae, presented by a point set at its boundary, a Gaussian mix-

ture model (GMM) registration algorithm is used to establish close correspondence across the training set [23]. To generate the mean shape for all the vertebrae and their transformations  $T_{n,l}$  to each instance generalized procrustes analysis is used.  $T_{n,l}$  represents the the similarity transformation from the  $l$ th vertebra of the mean shape to the corresponding vertebra of the  $n$ th instance. The PGs are extracted by concatenating the transformations for all anatomies. Assuming that shapes belong to Euclidean space, shape statistics are derived by directly applying the PCA analysis on points coordinates of the training set. Note that this analysis is performed on the entire ensemble (i.e., the entire lumbar vertebrae) [41].

The statistical shape+pose multi-vertebrae model is instantiated by applying different weights to the pose and shape PGs and combining them as follows:

$$s_l = \Phi(\omega^s, \omega^p) = \Phi_l^p(\Phi_l^s(\omega^s); \omega^p). \quad (6)$$

Here,  $\Phi_l^p(\cdot; \omega^p)$  and  $\Phi_l^s(\cdot)$  denote similarity transformation and a shape, respectively, which are built by a combination of the pose and shape PGs with corresponding weight using

$$\Phi_l^p(\cdot; \omega^p) = \mu_l^p \prod_{k=1}^K \exp(\omega_k^p v_{k,l}^p)$$

and

$$\Phi_l^s = \exp_{\mu_l^s} \left( \sum_{k=1}^K \omega_k^s \omega_{k,l}^s \right). \quad (7)$$

$\omega_k^s$  is the weight applied to the  $k$ th shape PG and  $\omega_k^p$  is the weight applied to the  $k$ th pose.

#### APPENDIX B

##### OPTIMIZED PHASE SYMMETRY BASED BONE SURFACE EXTRACTION

The PS metric, used for extraction of local phase bone features from US data, is obtained by convolving the US image with a 2-D Log-Gabor filter in the frequency domain [30]. The transfer function of a 2-D Log-Gabor filter ( $G_{ij}$ ), in the frequency domain can be constructed as

$$G_{ij} = \exp \left( - \frac{\log^2 \left( \frac{\omega}{\omega_{0j}} \right)}{2 \left( \log^2 \left( \frac{\kappa}{\omega_{0j}} \right) \right)} \right) \times \exp \left( - \frac{\theta - \theta_0}{2\sigma_\theta^2} \right). \quad (8)$$

Here, the subscripts  $i$  and  $j$  denote, respectively, the number of scales and orientations of the filter.  $\kappa$  is the standard deviation

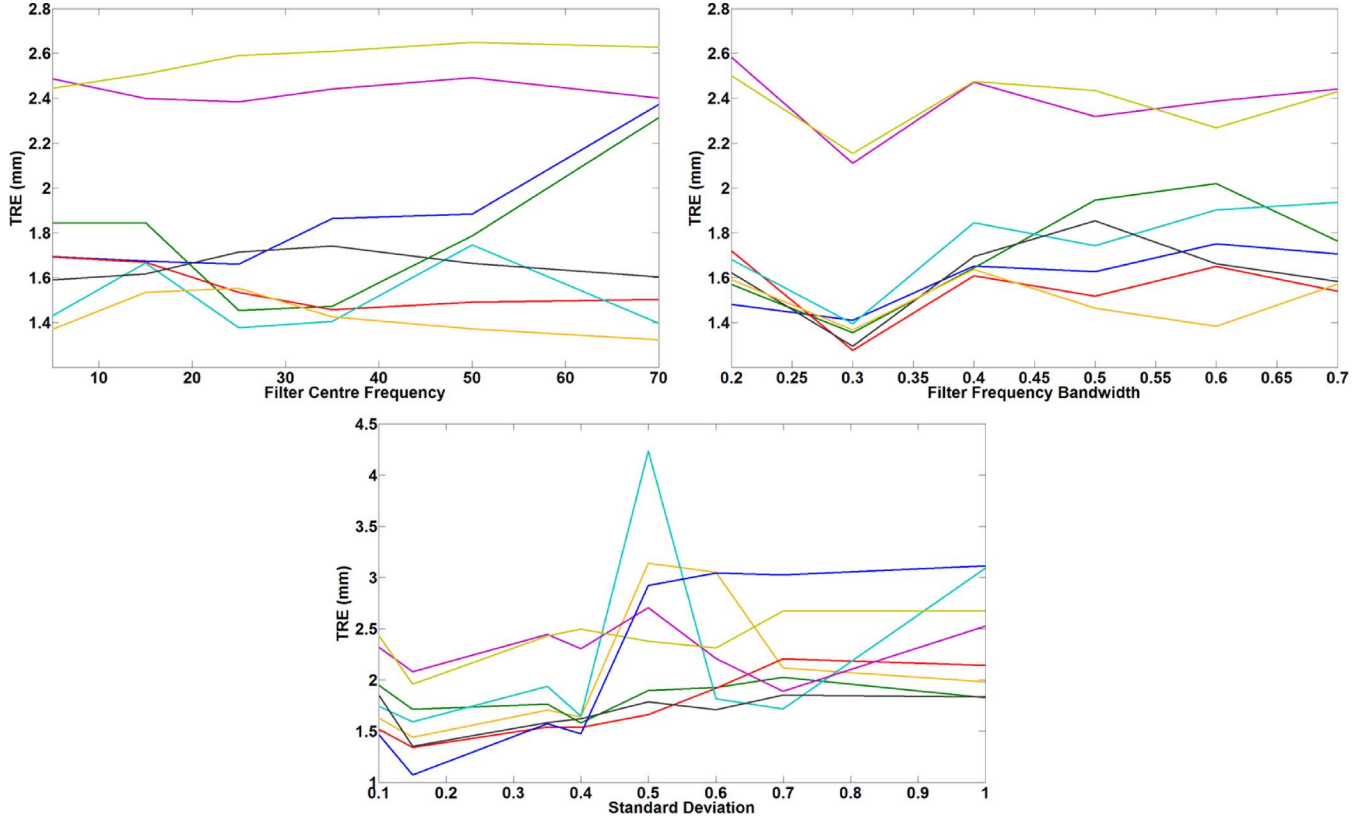


Fig. 8. Quantitative results showing the effect of LPT filter parameters [frequency bandwidth ( $\sigma_\omega$ ), filter center frequency ( $\kappa$ ) and standard deviation ( $\delta$ )] on the TRE. Plots are obtained using eight of the US volumes (denoted as eight different colored line plots) which were part of the exhaustive search optimization process.

of the filter in the radial direction and  $\omega_{0j}$  is the filter's center spatial frequency. The term  $\kappa/\omega$  is related to the bandwidth of the filter. The scaling of the filter is achieved by using different wavelengths that are based on multiples of a minimum wavelength  $\lambda_{\min}$ . The relationship between the filter scale  $j$  and filter center frequency  $\omega_0$  is given as:  $\omega_0 = 1/(\lambda_{\min}(\delta^{j-1}))$ , where  $\delta$  is a user defined scaling factor.  $\sigma_\theta$  is the standard deviation of the Gaussian spreading function in the angular direction that describes the filter's angular selectivity. The PS descriptor is obtained by combining the output of the Log-Gabor filter ( $G_{ij}$ ) using different scales and orientations

$$PS(x, y) = \frac{\sum_i \sum_j [|e_{ij}(x, y)| - |o_{ij}(x, y)|] - T_i}{\sum_i \sum_j \sqrt{e_{ij}^2(x, y) + o_{ij}^2(x, y)} + \varepsilon} \quad (9)$$

where  $e_{ij}^2(x, y)$  and  $o_{ij}^2(x, y)$  are obtained by inverse Fourier transforming the convolution results [30]. The  $[\cdot]$  operator denotes zeroing of any negative values and  $\varepsilon$  is a small positive constant used to avoid division by zero which was set to 0.001 [26], [30].  $T_i$  is a noise threshold value calculated for each orientation separately using the response of the smallest scale filter [30]. The filter parameters were automatically optimized using the framework proposed by Hacıhaliloglu *et al.* [30].

#### APPENDIX C

##### MONOGENIC FILTER BASED BONE SURFACE EXTRACTION

The monogenic filter was originally proposed by Felsberg and Sommer [43]. This representation preserves the core prop-

erties of the 1-D analytic signal that decomposes a signal into information about structure (local phase) and energy (local amplitude). The frequency domain representation of the monogenic filter is

$$MF = (US_B, US_B H_1(u_1, u_2), US_B H_2(u_1, u_2))$$

$$H_1(u_1, u_2) = i \frac{u_1}{\sqrt{u_1^2 + u_2^2}}, H_2(u_1, u_2) = i \frac{u_2}{\sqrt{u_1^2 + u_2^2}}. \quad (10)$$

The monogenic filter based FS descriptor is defined as

$$FS(x, y) = \sum_j \frac{[|even(x, y)| - |odd(x, y)|] - T_j}{\sqrt{even^2(x, y) + odd^2(x, y)} + \varepsilon}$$

where

$$even(x, y) = F^{-1}(US_B)$$

and

$$odd(x, y) = F^{-1}(\sqrt{(US_B H_1)^2 + (US_B H_2)^2}). \quad (11)$$

Here,  $F^{-1}$  denotes inverse Fourier transform operation and  $US_B$  band-pass filtered US image using Log-Gabor filter [28].

#### REFERENCES

- [1], Chartbook on trends in the health of Americans Nat. Center Health Stat., Hyattsville, MD, Tech. Rep., 2006.

- [2] H. Allen, D. Hubbard, and S. Sullivan, "The burden of pain on employee health and productivity at a major provider of business service," *J. Occupat. Environ. Med.*, vol. 47, no. 7, pp. 658–670, 2005.
- [3] S. Bevan, The impact of back pain on sickness absence in Europe 2012 [Online]. Available: <http://www.theworkfoundation.com>
- [4] M. L. Mahowald, J. A. Singh, and P. Majeski, "Opioid use by patients in an orthopedics spine clinic," *Arthritis Rheumatism*, vol. 52, no. 1, pp. 312–321, 2005.
- [5] T. Grau, R. W. Leibold, R. Conradi, E. Martin, and J. Motsch, "Efficacy of ultrasound imaging in obstetric epidural anesthesia," *J. Clin. Anesthesia*, vol. 14, no. 3, pp. 169–175, 2002.
- [6] D. Tran and R. Rohling, "Automatic detection of lumbar anatomy in ultrasound images of human subjects," *IEEE Trans. Biomed. Eng.*, vol. 57, no. 9, pp. 2248–2256, Sep. 2010.
- [7] C. Clarke, J. Moore, C. Wedlake, D. Lee, S. Ganapathy, M. Salbalbal, T. Wilson, T. Peters, and D. Bainbridge, "Virtual reality imaging with real-time ultrasound guidance for facet joint injections: A proof of concept," *Anesthesia Analgesia*, vol. 110, no. 5, pp. 1461–1463, 2010.
- [8] J. Moore, C. Clarke, D. Bainbridge, C. Wedlake, A. Wiles, D. Pace, and T. Peters, "Image guidance for spinal facet injections using tracked ultrasound," in *Med. Image Comput. Comput.-Assist. Intervent.*, 2009, vol. 5761, pp. 516–523.
- [9] E. C. S. Chen, P. Mousavi, S. Gill, G. Fichtinger, and P. Abolmaesumi, "Ultrasound guided spine needle insertion," in *Proc. SPIE Med. Imag.*, 2010, vol. 7625, pp. 762 538–762 538-8.
- [10] G. Penney, D. Barratt, C. Chan, M. Slomczykowski, T. Carter, P. Edwards, and D. Hawkes, "Cadaver validation of intensity-based ultrasound to CT registration," *Med. Image Anal.*, vol. 10, no. 3, pp. 385–395, 2006.
- [11] B. Brendel, S. Winter, A. Rick, M. Stockheim, and H. Ermert, "Registration of 3-D CT and ultrasound datasets of the spine using bone structures," *Comput. Aid. Surg.*, vol. 7, no. 3, pp. 146–155, 2002.
- [12] C. Yan, B. Goulet, J. Pelletier, S.-S. Chen, D. Tampieri, and D. Collins, "Towards accurate, robust and practical ultrasound CT registration of vertebrae for image-guided spine surgery," *Int. J. Comput. Assist. Radiol. Surg.*, vol. 6, no. 4, pp. 523–537, 2011.
- [13] S. Winter, I. Pechlivanis, C. Dekomien, C. Igel, and K. Schmieder, "Toward registration of 3-D ultrasound and CT images of the spine in clinical praxis: Design and evaluation of a data acquisition protocol," *Ultrasound Med. Biol.*, vol. 35, no. 11, pp. 1773–1782, 2009.
- [14] S. Gill, P. Abolmaesumi, G. Fichtinger, J. Boisvert, D. Pichora, D. Borschneck, and P. Mousavi, "Biomechanically constrained groupwise ultrasound to CT registration of the lumbar spine," *Med. Image Anal.*, vol. 16, no. 3, pp. 662–674, 2012.
- [15] S. Khallaghi, P. Mousavi, D. Borschneck, G. Fichtinger, and P. Abolmaesumi, "Biomechanically constrained groupwise statistical shape model to ultrasound registration of the lumbar spine," in *Inf. Process. Comput.-Assist. Intervent.*, 2011, vol. 6689, pp. 47–54.
- [16] A. Rasoulia, P. Abolmaesumi, and P. Mousavi, "Feature-based multi-body rigid registration of CT and ultrasound images of lumbar spine," *Med. Phys.*, vol. 39, no. 6, pp. 3154–3166, 2012.
- [17] D. Barratt, G. Penney, C. Chan, M. Slomczykowski, T. Carter, P. Edwards, and D. Hawkes, "Self-calibrating 3-D ultrasound-based bone registration for minimally invasive orthopedic surgery," *IEEE Trans. Med. Imag.*, vol. 25, no. 3, pp. 312–323, Mar. 2006.
- [18] A. Rasoulia, R. Rohling, and P. Abolmaesumi, "Augmentation of paramedian 3-D ultrasound images of the spine," in *Inf. Process. Comput.-Assist. Intervent.*, 2013, vol. 7915, pp. 51–60.
- [19] A. K. Jain and R. H. Taylor, "Understanding bone responses in B-mode ultrasound images and automatic bone surface extraction using a Bayesian probabilistic framework," in *Proc. SPIE Med. Imag.*, 2004, pp. 131–142.
- [20] J. Kowal, C. Amstutz, F. Langlotz, H. Talib, and M. G. Ballester, "Automated bone contour detection in ultrasound B-mode images for minimally invasive registration in computer-assisted surgery: An in vitro evaluation," *Int. J. Med. Robot. Comput. Assist. Surg.*, vol. 3, no. 4, pp. 341–348, 2007.
- [21] P. Foroughi, E. Boctor, M. Swartz, R. Taylor, and G. Fichtinger, "Ultrasound bone segmentation using dynamic programming," in *Proc. IEEE Ultrason. Symp.*, 2007, pp. 2523–2526.
- [22] M. Moghari and P. Abolmaesumi, "Point-based rigid-body registration using an unscented Kalman filter," *IEEE Trans. Med. Imag.*, vol. 26, no. 12, pp. 1708–1728, Dec. 2007.
- [23] A. Rasoulia, R. N. Rohling, and P. Abolmaesumi, "Group-wise registration of point sets for statistical shape models," *IEEE Trans. Med. Imag.*, vol. 31, no. 11, pp. 2025–2034, Nov. 2012.
- [24] D. Boukerroui, J. Noble, M. C. Robini, and M. Brady, "Enhancement of contrast regions in suboptimal ultrasound images with application to echocardiography," *Ultrasound Med. Biol.*, vol. 27, no. 12, pp. 1583–1594, 2001.
- [25] V. Grau and J. Noble, "Adaptive multiscale ultrasound compounding using phase information," in *Med. Image Comput. Comput.-Assist. Intervent.*, 2005, vol. 3749, pp. 589–596.
- [26] M. Mulet-Parada and J. Noble, "2-D+T acoustic boundary detection in echocardiography," *Med. Image Anal.*, vol. 4, no. 1, pp. 21–30, 2000.
- [27] K. Rajpoot, V. Grau, and J. Noble, "Local-phase based 3-D boundary detection using monogenic signal and its application to real-time 3-D echocardiography images," in *Proc. IEEE Int. Symp. Biomed. Imag. From Nano to Macro*, 2009, pp. 783–786.
- [28] B. Rahmatullah, A. Papageorgiou, and J. Noble, "Integration of local and global features for anatomical object detection in ultrasound," in *Med. Image Comput. Comput.-Assist. Intervent.*, 2012, vol. 7512, pp. 402–409.
- [29] I. Hacıhaliloglu, R. Abugharbieh, A. J. Hodgson, and R. N. Rohling, "Bone surface localization in ultrasound using image phase based features," *Ultrasound Med. Biol.*, vol. 35, no. 9, pp. 1475–1487, 2009.
- [30] I. Hacıhaliloglu, R. Abugharbieh, A. J. Hodgson, and R. N. Rohling, "Automatic adaptive parameterization in local phase feature-based bone segmentation in ultrasound," *Ultrasound Med. Biol.*, vol. 37, no. 10, pp. 1689–1703, 2011.
- [31] I. Hacıhaliloglu, R. Abugharbieh, A. J. Hodgson, R. N. Rohling, and P. Guy, "Automatic bone localization and fracture detection from volumetric ultrasound images using 3-D local phase features," *Ultrasound Med. Biol.*, vol. 38, no. 1, pp. 128–144, 2012.
- [32] A. Brounstein, I. Hacıhaliloglu, P. Guy, A. Hodgson, and R. Abugharbieh, "Towards real-time 3-D US to CT bone image registration using phase and curvature feature based GMM matching," in *Medical Image Comput. Comput.-Assist. Intervent.*, 2011, vol. 6891, pp. 235–242.
- [33] I. Hacıhaliloglu, A. Rasoulia, R. N. Rohling, and P. Abolmaesumi, "Statistical shape model to 3-D ultrasound registration for spine interventions using enhanced local phase features," in *Med. Image Comput. Comput.-Assist. Intervent.*, 2013, vol. 8150, pp. 361–368.
- [34] M. C. Morrone and R. A. Owens, "Feature detection from local energy," *Pattern Recogn. Lett.*, vol. 6, no. 5, pp. 303–313, Dec. 1987.
- [35] M. Felsberg and U. Kothe, "GET: The connection between monogenic scale-space and Gaussian derivatives," in *Proc. Scale Space Conf. Gaussian Derivatives*, 2005, pp. 192–203.
- [36] U. Kothe and M. Felsberg, "Riesz-transforms vs. derivatives: On the relationship between the boundary tensor and the energy tensor," in *Proc. Scale Space Conf. Gaussian Derivatives*, 2005, pp. 179–191.
- [37] P. M. Simon, A. E. Orias, G. B. Andersson, H. S. An, and N. Inoue, "In vivo topographic analysis of lumbar facet joint space width distribution in healthy and symptomatic subjects," *Spine*, vol. 37, no. 12, pp. 1058–1064, 2012.
- [38] S. Fyreface-Ogan, Anatomy and clinical importance of the epidural space, epidural analgesia—Current views and approaches 2012 [Online]. Available: <http://www.intechopen.com/books/epidural-analgesia-current-views-and-approaches/anatomy-and-clinical-importance-of-the-epidural-space>
- [39] A. Amir-khalili, A. J. Hodgson, and R. Abugharbieh, "Real-time extraction of local phase features from volumetric medical image data," in *Proc. IEEE Int. Symp. Biomed. Imag. From Nano to Macro*, 2013, pp. 930–933.
- [40] P. Fletcher, C. Lu, and S. Joshi, "Statistics of shape via principal geodesic analysis on lie groups," in *Proc. IEEE Comput. Soc. Conf. Comput. Vis. Pattern Recognit.*, 2003, vol. 1, pp. 95–101.
- [41] A. Rasoulia, R. Rohling, and P. Abolmaesumi, "A statistical multi-vertebrae shape+pose model for segmentation of CT images," in *Proc. SPIE-Med. Imag.*, 2013, pp. 86 710–86 710P-6.
- [42] M. Bossa and S. Olmos, "Multi-object statistical pose+shape models," in *Proc. IEEE Int. Symp. Biomed. Imag. From Nano to Macro*, 2007, pp. 1204–1207.
- [43] M. Felsberg and G. Sommer, "The monogenic signal," *IEEE Trans. Signal Process.*, vol. 49, no. 12, pp. 3136–3144, Dec. 2001.